Inorganic Chemistry

Article

pubs.acs.org/IC

Characterization and Luminescence Properties of Lanthanide-Based Polynuclear Complexes Nanoaggregates

François Le Natur,[†] Guillaume Calvez,*[,†] Jean-Paul Guégan,[‡] Laurent Le Pollès,[‡] Xavier Trivelli,[∥] Kevin Bernot,[†] Carole Daiguebonne,[†] Chrystelle Neaime,[†,§] Karine Costuas,[§] Fabien Grasset,[§,⊥] and Olivier Guillou*[,†]

[†]INSA, [‡]ENSCR, and [§]Université de Rennes 1, UMR 6226 Institut des Sciences Chimiques de Rennes, F-35708 Rennes, France

[∥]Université Lille 1—Sciences et Technologies, UMR CNRS 8576 UGSF, IFR 147—FRE 3637, F-59655 Villeneuve d'Ascq, France

Supporting Information

ABSTRACT: For the first time, hexanuclear complexes with general chemical formula $[Ln_6O(OH)_8(NO_3)_6(H_2O)_n]^{2+}$ with n = 12 for Ln = Sm−Lu and Y and n = 14 for Ln = Pr and Nd were stabilized as nanoaggregates in ethylene glycol (EG). These unprecedented nanoaggregates were structurally characterized by ^{89}Y and ^{1}H NMR spectroscopy, UV−vis absorption and luminescence spectroscopies, electrospray ionization mass spectrometry, diffusion ordered spectroscopy, transmission electron microscopy, and dynamic light scattering. These nanoaggregates present a 200 nm mean solvodynamic diameter. In these nanoaggregates, hexanuclear complexes are isolated and solvated by EG molecules. The replacement of ethylene glycol by 2-hydroxybenzyl alcohol provides new nanoaggregates that present an antenna effect toward lanthanide ions. This results in a significant enhancement of the luminescence properties of the aggregates and demonstrates the suitability of the strategy for obtaining highly tunable luminescent solutions.

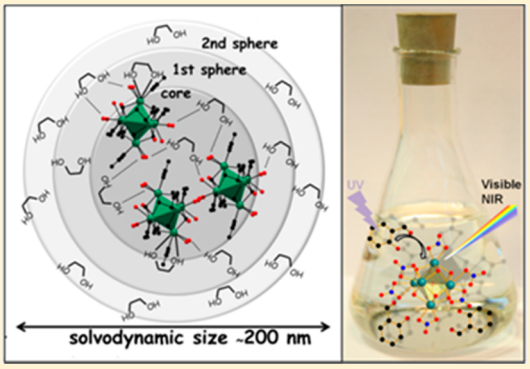

INTRODUCTION

Lanthanide-based luminescent materials attract increasing attention because of their potential interest in a wide range of applications[1] such as lighting,[2,3] liquid-crystal engineering,[4] or fluoro-immunoassays.[5,6] A lot of work has been devoted to lanthanide mononuclear complexes because their rational design constitutes an advantage. However, their susceptibility to quenching effects caused by water or hydroxyl groups is a drawback for such complexes.[7] Besides, lanthanide-based nanoparticles have also attracted attention[8] because they exhibit long luminescence lifetimes and are not sensitive to particle size.[9−11] The main drawback of this class of compounds is that their size can only be controlled within a certain range resulting in materials with particle size distributions. Oligonuclear lanthanide complexes are located between these two limits: they are much larger than mononuclear complexes but still present well-defined sizes and compositions.

To date, several lanthanide-based hydroxo polynuclear complexes have been reported that present a nuclearity ranging from 2 to 60.[12−37] Most of these complexes have been prepared by one-pot synthetic methods and cannot be used as molecular precursors for designing new materials because of their low stability and solubility. For a decade our group has been involved in the synthesis and characterization of hexanuclear rare earth-based complexes[27,38−40] with general chemical formula $[Ln_6O(OH)_8(NO_3)_6(H_2O)_n]^{2+}$ with n = 12 for Ln = Sm−Lu and Y and n = 14 for Ln = Pr and Nd. These complexes crystallize in different polymorphic phases depending on the synthetic route and on the involved lanthanide ion.[38,41,42] Whatever the crystalline phase is, the hexanuclear complex is the same (Figure 1). It consists of a quasi-perfect octahedron with a lanthanide ion on each apex and a μ_6-O^{2-} at the center. Each face of the octahedron is capped by a μ_3-OH^- group. Additionally, each lanthanide is bound to a bidentate NO_3^- ion and two coordination water molecules. For the biggest lanthanide ions (Pr and Nd) two of the six lanthanide ions are linked to a third coordination water molecule.[38]

These complexes have been proved to be usable as molecular precursors,[41] and coordination polymers in which they act as metallic centers have been synthesized and structurally characterized.[43] These coordination polymers exhibit unique luminescence properties.[44,45]

Despite these promising results, it must be noticed that these hexanuclear complexes present weak stability in moist media and in most usual polar organic solvents (see Supporting Information, Table S1).[41] In these media, hydrolysis of the complexes occurs and leads to insoluble polymeric hydroxides. Therefore, the complexes can conveniently be used as molecular precursors only in acetonitrile or alcohols. However,

Received: April 27, 2015
Published: May 29, 2015

DOI: 10.1021/acs.inorgchem.5b00947
Inorg. Chem. 2015, 54, 6043−6054

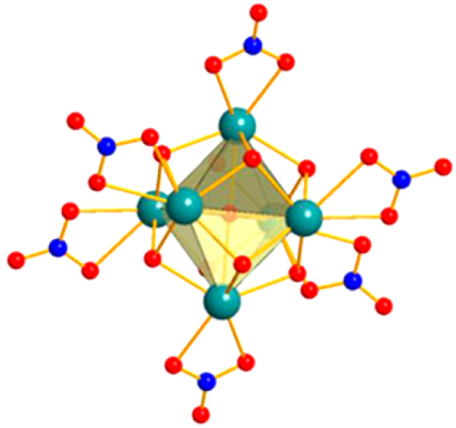

Figure 1. Hexanuclear complexes $[Ln_6O(OH)_8(NO_3)_6(H_2O)_{12}]^{2+}$ with Ln = Sm−Lu and Y. Coordination water molecules were omitted for clarity. Redrawn from ref 43.

hexanuclear complexes present quite low solubility in these solvents, and saturated solution in CH_3CN exhibits weak luminescence that is not visible to the naked eye.

Another drawback is the quite moderate stability of the hexanuclear cores toward strong coordinating ligands.[39,46] All these observations have encouraged us to find another solvent in which the solubility and the stability of the hexanuclear complexes would be improved. Polyols revealed to be good candidates, and interesting results were obtained especially with ethane-1,2-diol (ethylene glycol), hereafter symbolized by EG.

The choice of this solvent was motivated by several considerations: (i) alcohol groups can substitute coordination water molecules and establish coordination bonds with the lanthanide ions;[47] (ii) they can also be involved in hydrogen bonds with coordination water molecules and/or capping hydroxide groups; (iii) EG is known, in food industry, for its ability to protect against water,[48,49] which could be an asset for these moisture-sensitive complexes; (iv) some EG-based lanthanide complexes have already been described,[50−57] even in the solid state;[58,59] (v) 50:50 mixtures of EG/ethanol are liquid over a large temperature range (−50 to +100 °C),[60] which is an asset as far as luminescent solutions with potential applications are targeted.

We report here the synthesis and the characterization of the first nanoaggregates of hexanuclear complexes in EG, hereafter symbolized by $[Ln_6]^{2+}$@EG. Their fine structural characterization requires the use of various techniques such as electrospray ionization mass spectrometry (ESI-MS), ^{1}H diffusion ordered spectroscopy (DOSY) NMR, transmission electron microscopy (TEM), dynamic light scattering (DLS), and luminescence and ^{89}Y NMR liquid-state spectroscopies. The general character of this strategy was validated by using an aromatic polyol, namely, 2-hydroxybenzyl alcohol (HBA), that can favor lanthanide emission through antenna effects. These nanoaggregates are hereafter symbolized by $[Ln_6]^{2+}$@HBA. Some of the members of this second family exhibit interesting luminescence properties demonstrating the suitability of this synthetic strategy for preparing highly tunable luminescent solutions.

EXPERIMENTAL SECTION

Synthesis of $[Ln_6]^{2+}$@EG Entities. Lanthanide oxides were purchased from A.M.P.E.R.E Industrie and used without further purification. Hydrated lanthanide nitrates were prepared from the corresponding oxides according to literature methods.[61] Microcrystalline powders of lanthanide hexanuclear complexes with general chemical formula of $[Ln_6O(OH)_8(NO_3)_6(H_2O)_n]\cdot 2NO_3\cdot 2H_2O$ with n = 12 for Ln = Sm−Lu and Y and n = 14 for Ln = Pr or Nd (hereafter symbolized by $[Ln_6]^{2+}$) were synthesized by direct hydrolysis of the corresponding nitrates according to an already reported process.[41] Microcrystalline powders were characterized by X-ray powder diffraction and thermal analyses.

Saturated EG solutions of the hexanuclear complexes were prepared by dissolving 150 mg of a microcrystalline powder of $[Ln_6O(OH)_8(NO_3)_6(H_2O)_n]\cdot 2NO_3\cdot 2H_2O$ with n = 12 for Ln = Sm−Lu and Y and n = 14 for Ln = Pr or Nd in 3 mL of EG under vigorous stirring at 40 °C. After they cooled, the mixtures were centrifuged (13 000 rpm) for 5 min and filtered. The Ln^{3+} content of the obtained clear solutions was estimated by complexometric titration with ethylenediaminetetraacetic acid.[62] Whatever the lanthanide ion was, the solubility of $[Ln_6]^{2+}$ complexes was 0.03 mol L^{-1} (roughly 45 g L^{-1}, depending on the involved lanthanide ion). Notice that this solubility is greater than those observed in usual organic solvents.

Synthesis of $[Ln_6]^{2+}$@HBA Entities. A microcrystalline powder (100 mg, ∼0.05 mmol) of $[Ln_6O(OH)_8(NO_3)_6(H_2O)_n]\cdot 2NO_3\cdot 2H_2O$ with n = 12 for Ln = Sm−Lu and Y and n = 14 for Ln = Nd is added to a solution of HBA (0.6M) in 10 mL of ethanol that was previously dried on molecular sieves (4 Å). This mixture is refluxed for 1 h. Solid microcrystalline powder dissolves progressively during this time. The mixture is then cooled and filtered for eliminating insoluble materials. Then, the obtained clear solution is evaporated to dryness at 40 °C. The obtained solid is dissolved again in ethanol, and the residual solid is filtered again. The finally obtained pale yellow solution will be hereafter referred to as $[Ln_6]^{2+}$@HBA. Hexanuclear complexes content was estimated to be 0.006 mol L^{-1}, which is 5 times less than that for $[Ln_6]^{2+}$@EG.

Liquid-State ^{89}Y NMR Measurements. Recent papers prove that ^{89}Y NMR is a useful probe of local ordering in solid state[63−67] and liquid state.[68] Nevertheless, ^{89}Y is still far from being a routine nucleus because of its characteristics (rather low sensitivity and long T_1 relaxation time), which constitute serious drawbacks in terms of NMR techniques and lead to time-consuming NMR experiments since they are based on conventional pulse sequences.[69] Diamagnetic lanthanide ions were chosen for achieving high-resolution solid-state NMR experiments.

The ^{89}Y NMR experiments were recorded on Avance 400 MHz and Avance III 900 MHz equipped with 5 mm broad-band direct probes at 323 K. The experiments presented in this paper were recorded at 9.4 T using a UDEFT sequence.[70] It appears that, after a careful optimization of the UDEFT sequence, a moderate (9.4 T) magnetic field is sufficient to provide good-quality NMR spectra in liquid-state ^{89}Y NMR. At 9.4 T (^{1}H = 400 MHz), ^{89}Y resonates at a Larmor frequency of 19.6 MHz. The 90° ^{89}Y pulse was calibrated on a $Y(NO_3)_3$ 1 mol L^{-1} in D_2O (24 μs). All the ^{89}Y chemical shift values are referenced against YCl_3 1 mol L^{-1} in D_2O. More detailed experimental parameters are described in the Supporting Information.

Liquid state ^{1}H Diffusion Ordered Spectroscopy NMR Measurements. ^{1}H NMR spectra were recorded on a BrukerAvance III 400 spectrometer (400.13 MHz for ^{1}H) equipped with a BBFO probe, Z-gradient coil, and a GREAT 1/10 gradient unit. ^{1}H DOSY NMR experiments were performed using standard conditions (further details can be found in Supporting Information).

Other Characterization Techniques. X-ray powder diffraction, TEM, DLS, ESI-MS, colorimetric and optical measurements, and other experimental details are reported in Supporting Information.

RESULTS AND DISCUSSION

Characterization of $[Ln_6]^{2+}$@EG Aggregates. Hexanuclear complexes were prepared as microcrystalline powders according to a procedure that has been described elsewhere.[41] Solid-state UV−vis absorption, excitation, and emission spectra were measured to be used as references (see Supporting Information, Figures S1 and S2). Intrinsic quantum yields

DOI: 10.1021/acs.inorgchem.5b00947
Inorg. Chem. 2015, 54, 6043−6054

(Q_{Ln}^{Ln}) and observed lifetimes (τ_{obs}) were measured for the Sm-, Eu-, Tb-, and Dy-containing compounds. Results are listed in Table 1.

Table 1. Solid-State Intrinsic Quantum Yields and Observed Lifetimes for $[Ln_6O(OH)_8(NO_3)_6(H_2O)_{12}]\cdot 2NO_3\cdot 2H_2O$ for Ln = Sm, Eu, Tb, Dy

Ln	λ_{exc} (nm)	Q_{Ln}^{Ln} (%)	τ_{obs} (ms)
Sm	404	0.14(2)	$6.8(1).10^{-3}$
Eu	394	7.6(7)	0.19(2) - 0.22(2)*
Tb	379	29(3)	0.74(7)
Dy	376	0.31(3)	$9.2(1).10^{-3}$

*Measured at 77 K.

These microcrystalline powders are then dissolved in EG. Clear saturated solutions (0.03 mol L^{-1}) are obtained. First these solutions were evaporated to dryness (100 °C). Powder X-ray diffraction diagrams of the resulting microcrystalline powders were recorded and compared to experimental and calculated from the solid-state crystal structure powder X-ray diffraction patterns (Supporting Information, Figure S3). These experiments demonstrate that hexanuclear complexes are unchanged after the dissolution/recrystallization process.

To evaluate the stability of the hexanuclear assemblies in the liquid state we recorded liquid-state ^{89}Y NMR spectra of $[Y_6O(OH)_8(NO_3)_6(H_2O)_{12}]\cdot 2NO_3\cdot 2H_2O$ and of $Y(NO_3)_3\cdot 6H_2O$ dissolved in EG (Figure 2).

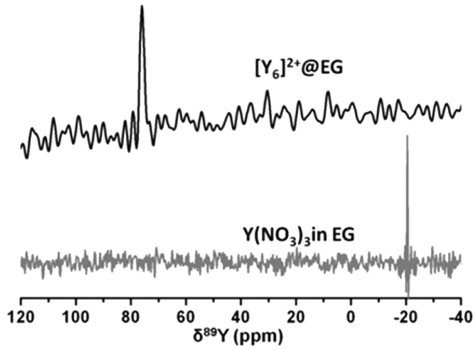

Figure 2. ^{89}Y (19.6 MHz) liquid-state NMR spectra of $[Y_6]^{2+}$@EG (upper) and of $Y(NO_3)_3\cdot 6H_2O$ (lower) in EG at 50 °C (reference aqueous YCl_3 1 mol L^{-1}). The number of scans for $[Y_6]^{2+}$@EG was fixed to 1000 (acquisition time: 0.5 d).

The spectrum recorded for $[Y_6]^{2+}$@EG shows only one peak at 78 ppm. This peak is 100 ppm away from the one of $Y(NO_3)_3\cdot 6H_2O$ dissolved in EG. The chemical shift value observed for $[Y_6]^{2+}$@EG is in the same range as the isotropic chemical shifts observed, in the solid state, by ^{89}Y CPMAS NMR experiments for a structurally related hexanuclear yttrium compound (50 to 60 ppm for three inequivalent yttrium positions in the hexanuclear entity in solution).[44] In solution, the contributions of the three different crystallographic sites existing in the solid state are averaged by molecular dynamics.[44] These results strongly suggest that there is only one species in solution presenting an isotropic chemical shift consistent with existence of an hexanuclear $[Y_6]^{2+}$ entity and that the yttrium-containing species in solution are clearly different from an isolated Y^{3+} ion.

Because of the high viscosity of the $[Eu_6]^{2+}$@EG solution (16.9 cP at 20 °C) we performed an ESI-MS spectrum of a diluted solution of $[Eu_6]^{2+}$@EG in propan-2-one (1/100). In this spectrum, no peak corresponds to a simple $[Eu_6]^{2+}$ complex, and the main peak is centered on the value m/z = 949 (305 ppm), which corresponds to the chemical formula $\{[Eu_6O(OH)_8(NO_3)_6(H_2O)_{12}] + 4\ EG\}^{2+}$. The peak that has been simulated using ChemCalc[71] software on the basis of this chemical formula is in reasonable agreement with experimental peak pattern (Supporting Information, Figure S4).

Dynamic light scattering experiments were also performed for saturated (C_0 = 0.03 mol L^{-1}) and diluted solutions of $[Y_6]^{2+}$@EG. These experiments reveal a large distribution of sizes centered at 200 nm that is not affected by dilution (see Figure 3). This observation is confirmed by a TEM picture that shows quite large spherical species (100 nm ≤ diameter ≤ 450 nm). These spherical entities present a sort of fogging that suggests a low metallic content.

These experiments suggest that hexanuclear complexes are solvated by EG molecules and aggregated. This phenomenon has already been observed for polyoxometallates[72] and gold nanoparticles.[73] The observed low metallic density seems to indicate that the hexanuclear entities are quite far from each other, and therefore the cohesion of the nanoaggregates could be attributed to a hydrogen-bond network that would involve EG molecules, water molecules, coordinated nitrate anions, and capping hydroxide groups.

These nanoaggregates do not induce turbidity:[74] the saturated solutions of $[Ln_6]^{2+}$@EG are limpid (Figure 4), and their liquid-state absorption spectra are free from noise (Supporting Information, Figure S5).

Because luminescent properties are targeted, we recorded excitation and emission spectra for $[Ln_6]^{2+}$@EG where Ln = Sm, Eu, Tb, Dy, that is, lanthanide ions that usually emit in the visible domain. These spectra are reported in Figure 4. They are quite similar to those recorded in the solid state. As expected, no antenna effect is observed, and luminescence is obtained by direct excitation of the lanthanide ions. Despite rather low luminance values (see Table 2) Eu- and Tb-containing solutions exhibit quite interesting luminescence (Figure 4). Sm- and Dy-based solutions present almost no luminescence. Therefore, their colorimetric coordinates and luminance were not measured (Table 2).

It is well-established that luminescence spectra of Eu-based compounds depend on the Eu^{3+} ion environment and can provide useful structural information. We thus study $[Eu_6]^{2+}$@EG in more detail. Luminescence spectra of both $[Eu_6]^{2+}$@EG and a solution of $Eu(NO_3)_3\cdot 6H_2O$ in EG are reported in Figure 5.

From this figure, it can be noticed that the Eu-based hexanuclear complex presents an emission spectrum that is quite different from the one of an isolated Eu^{3+} ion in EG. Moreover, comparison between the solid-state luminescence spectrum of $[Eu_6(\mu_6\text{-}O)(\mu_3\text{-}OH)_8(H_2O)_{12}(NO_3)_6]\cdot 2NO_3\cdot 2H_2O$ and the liquid-state luminescence spectrum of $[Eu_6]^{2+}$@EG (see Figure 6) suggests that the lanthanide ion environment is modified in solution.

The f-shell electrons of lanthanide ions are influenced by their ligand environment especially via electrostatic interactions.[75] This influences their fluorescence response.[76−78] In the present case, the presence of lanthanide ions in the coordination sphere can create enhanced electrostatic effects compared to main group atoms. To evaluate this influence of

DOI: 10.1021/acs.inorgchem.5b00947
Inorg. Chem. 2015, 54, 6043−6054

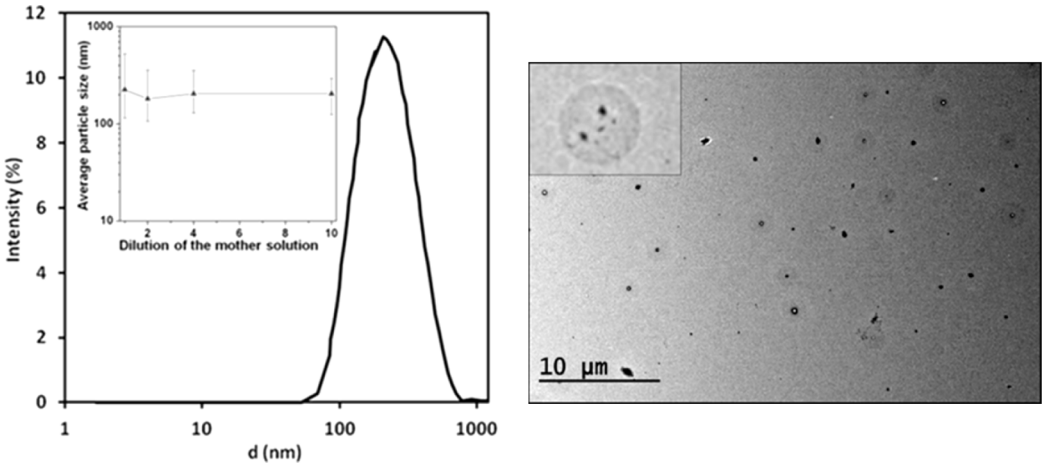

Figure 3. (left) Analysis of the size of entities by DLS. Viscosity of the mother solution is 16.9(5) cP at 20 °C. (inset) Average particle size vs dilution of $[Y_6]^{2+}$@EG. (right) TEM picture of a diluted ($C_0/2$) solution of $[Y_6]^{2+}$@EG. The poor quality of the picture can be related to the presence of EG. (inset) Enlarged view of nanoaggregate (mean diameter: 220 nm).

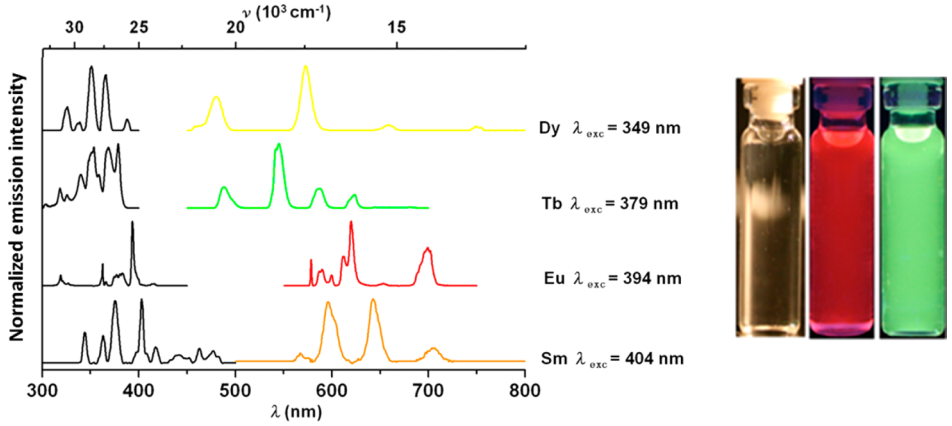

Figure 4. (left) Normalized excitation and emission spectra of $[Ln_6]^{2+}$@EG where Ln = Sm, Eu, Tb, or Dy. Individual spectra are reported in Supporting Information, Figure S6. (right) Pictures under visible light of $[Tb_6]^{2+}$@EG (left) and under UV irradiation (λ_{exc} = 365 nm) of $[Eu_6]^{2+}$@EG (middle) and $[Tb_6]^{2+}$@EG (right).

Table 2. Liquid-State Intrinsic Quantum Yields and Observed Lifetimes, Colorimetric Coordinates, and Luminance for $[Ln_6]^{2+}$@EG where Ln = Sm, Eu, Tb, or Dy

Ln	λ_{exc} (nm)	Q_{Ln}^{Ln} (%)	τ_{obs} (ms)	x^c	y^c	L^c (Cd·m^{-2})
Sm	404	0.19(2)	$5.4(1) \times 10^{-3}$			
Eu	394	12(1)	0.41(1)–0.40(1)[a]	0.65(1)	0.35(1)	0.037(1)
Eu[b]	394	83(8)	2.01(7)			
Tb	379	16(2)	1.00(4)	0.35(1)	0.57(1)	0.182(2)
Dy	376	0.02(1)	$1.4(1)\ 10^{-3}$			

[a]Measured at 77 K. [b]$[Ln_6]^{2+}$@EG-d_6; [c]Colorimetric and luminance measurements were performed under UV irradiation produced by a commercial lamp centered at 365 nm.

the Eu^{3+} environment onto its luminescence properties, quantum chemical calculations at the density functional theory (DFT) level were performed (see Supporting Information for computational details). On one hand, $Eu(H_2O)_4(NO_3)_3$[79] was considered as archetype of usual Eu^{3+} inorganic species for sake comparison. On the other hand, taking into account that a full treatment of the Eu_6 entity cannot be done, a model system, namely, $[EuLu_5(\mu_6\text{-}O)(\mu_3\text{-}OH)_8(H_2O)_{12}(NO_3)_6]^{2+}$ was taken to keep electrostatic interactions of the surrounding lanthanide ions onto the Eu^{3+} electronic structure.[80]

The study of the electronic structures represented in Figure 7 reveals in each case a split of the f-shell of the α-spin orbitals and of the β-spin orbitals unoccupied orbitals, mainly due to electrostatic effects. In the case of $[EuLu_5(\mu_6\text{-}O)(\mu_3\text{-}OH)_8(H_2O)_{12}(NO_3)_6]^{2+}$, a more pronounced admixture with the surrounding oxygen atomic orbitals of the ligand is observed (see Figure 7). Because of electrostatic interaction induced by vicinity of the other lanthanide motives, those are in the same region of energy as the f-levels of the Eu^{3+}. Even if DFT cannot be used as a quantitative tool, the comparison between the results obtained for $Eu(H_2O)_4(NO_3)_3$ and for the model $[EuLu_5(\mu_6\text{-}O)(\mu_3\text{-}OH)_8(H_2O)_{12}(NO_3)_6]^{2+}$ allows the drawing of qualitative conclusions. Here, we can deduce that there is a stronger influence of the environment on the electronic

DOI: 10.1021/acs.inorgchem.5b00947
Inorg. Chem. 2015, 54, 6043−6054

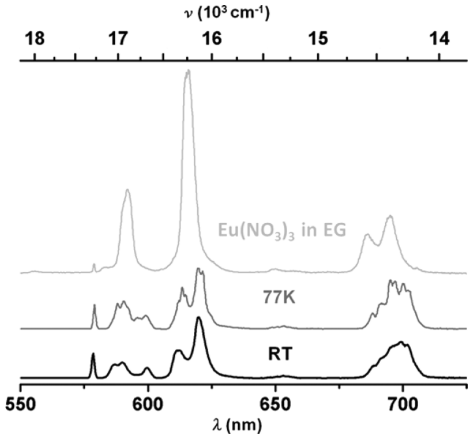

Figure 5. Room-temperature luminescence spectrum of a $Eu(NO_3)_3 \cdot 6H_2O$ solution in EG (upper). Room- and liquid nitrogen-temperature luminescence spectra of $[Eu_6]^{2+}$@EG (lower). All spectra were recorded under similar experimental conditions. λ_{exc} = 396 nm corresponds to the maximum of the excitation spectra ($^5L_6 \leftarrow {}^7F_0$ transition). Emission spectra were normalized on the basis of the $^5D_0 \rightarrow {}^7F_1$ transition ($\lambda_{em} \approx 590$ nm), which is dipolar magnetic and not sensitive to environment.[7] Normalized intensities are listed in Supporting Information, Table S2.

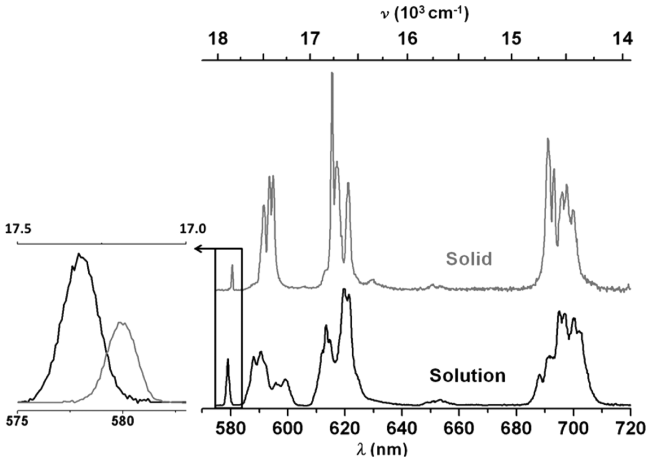

Figure 6. Normalized solid-state luminescence spectrum of $[Eu_6(\mu_6\text{-}O)(\mu_3\text{-}OH)_8(H_2O)_{12}(NO_3)_6]\cdot 2NO_3\cdot 2H_2O$ (77 K) and liquid-state luminescence spectrum of $[Eu_6]^{2+}$@EG. Normalizations were made on the basis of the peaks that correspond to dipolar magnetic $^5D_0 \rightarrow {}^7F_1$ transitions. (inset) Superimposition of the peaks that correspond to the $^5D_0 \rightarrow {}^7F_0$ transition. Integrated intensities are listed in Supporting Information, Table S3.

structure of the Eu^{3+} ion in the lanthanide cluster than in $Eu(H_2O)_4(NO_3)_3$. Furet and co-workers already showed such type of electrostatic ligand effects on the electronic structures of diverse monolanthanide systems.[75] Interestingly, one α-spin orbital is even found within the f-block. This surely modifies the energies of the first excited states and consequently the emission pattern. The calculated first septet excited states of the two compounds are ranging within the textbook values of the so-called Dieke diagrams.[7] For $Eu(H_2O)_4(NO_3)_3$, they are calculated at 1257, 1468, 2453, 4478, 5150, and 5231 cm^{-1} and are essentially f−f in character, but the populated level has 38% of oxygen character. Interestingly, 11 septet excited states are calculated for $[EuLu_5(\mu_6\text{-}O)(\mu_3\text{-}OH)_8(H_2O)_{12}(NO_3)_6]^{2+}$ in the same energy region (at 492, 728, 1097, 2605, 3182, 3499, 4023, 4217, 4441, 4763, 5092 cm^{-1}) and are separated from the others by more than 6000 cm^{-1}. A detailed description of the nature of those excited states is given in Supporting Information. An important feature is that the presence of oxygen-centered molecular orbitals closer to (and possibly intercalated in) the f-block compared to $Eu(H_2O)_4(NO_3)_3$ gives rise to additional excited states in the same energy region than the usual ones issued from pure f−f transitions. The associated oscillator strengths of those excitations are calculated to be larger, rendering them more probable to be populated. This could explain the unusually intense "$D_0 \rightarrow F_0$" peak observed experimentally since they are in the same energy range as the F_0 states.

These experiments and calculations demonstrate that luminescence spectrum of $[Eu_6]^{2+}$@EG can be used as a fingerprint of the hexanuclear complex in EG. Such modifications of the Eu^{3+} luminescence are used nowadays to titrate anions in water or in biological media.[81−83]

The emission spectrum of a saturated solution of the Eu-based hexanuclear complex in deuterated EG ($[Eu_6]^{2+}$@EG-d_6) was also measured, and its luminescence lifetime and intrinsic quantum yields were evaluated (see Table 2). Notice that the quantum yield is greatly enhanced in EG-d_6 (Q_{Eu}^{Eu} = 83%) and the luminescent lifetime as well (τ_{obs} = 2.0 ms). This suggests that some EG-d_6 enter in the first coordination sphere of the lanthanide ions. On the basis of these experiments it is possible to estimate the number of O−H vibrators replaced by O−D vibrators in the first coordination sphere with the following equation:[6,84−87]

$$q = A(k_{obs}^{O-H} - k_{obs}^{O-D})$$
$$\text{with } k_{obs}^{O-H} = \frac{1}{\tau_{obs}^{O-H}} \text{ and } k_{obs}^{O-D} = \frac{1}{\tau_{obs}^{O-D}} \quad (1)$$

where k_{obs}^{O-H} and k_{obs}^{O-D} are the kinetic constants in EG and in EG-d_6, respectively, A is an empirical factor (1.05 H_2O/ms for Eu^{3+}), and $2q$ is the number of O−H vibrators that were replaced in the first coordination sphere.[88] In the present system, this calculation leads to four O−H vibrators in the first coordination sphere. This value is in good agreement with the chemical formula of the starting hexanuclear complex. Most probably, one must consider that there is a dynamic exchange between EG and water molecules in the first coordination sphere of the lanthanide ions. However, this result must be taken into account with great care because this relationship has been established for aqueous solutions.

As explained above, TEM pictures also suggest that hexanuclear complexes are far away from each other. It is also well-known that intermetallic energy transfer is efficient when lanthanide ions are less than ∼10 Å far from each other.[63,89]

Spectrometric and colorimetric measurements of a series of compounds hereafter symbolized by $\{[Eu_6]_{1-x}^{2+}[Tb_6]_x^{2+}\}$@EG were performed. These compounds result from the dissolution in EG of mixtures of microcrystallines powders of $[Eu_6(\mu_6\text{-}O)(\mu_3\text{-}OH)_8(H_2O)_{12}(NO_3)_6]\cdot 2NO_3\cdot 2H_2O$ and $[Tb_6(\mu_6\text{-}O)(\mu_3\text{-}OH)_8(H_2O)_{12}(NO_3)_6]\cdot 2NO_3\cdot 2H_2O$ in variable ratios according to the dissolution process described above. The relative contents in Eu and Tb of the solutions are reported in Supporting Information, Table S4. The luminescence spectra and colorimetric measurements recorded under UV irradiation at 379 nm are reported in Figure 8. This wavelength is suitable

DOI: 10.1021/acs.inorgchem.5b00947
Inorg. Chem. 2015, 54, 6043−6054

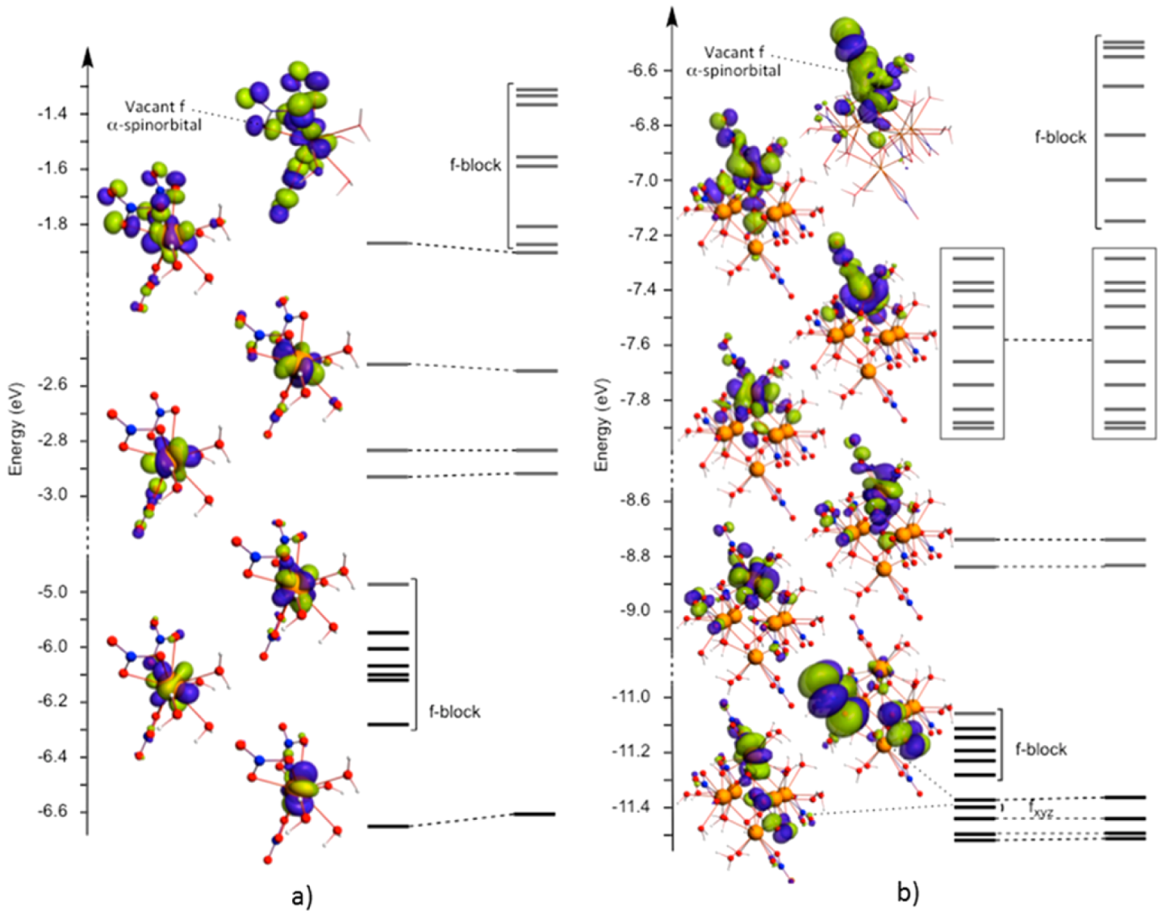

Figure 7. Molecular spinorbital diagram of (a) $Eu(H_2O)_4(NO_3)_3$ and (b) $[EuLu_5(\mu_6\text{-}O)(\mu_3\text{-}OH)_8(H_2O)_{12}(NO_3)_6]^{2+}$. Gray levels are empty. The highest occupied α-spinorbitals and the first empty one are represented (contour values: (a) ± 0.03 (e $Bohr^3)^{1/2}$ and (b) 0.02 (e $Bohr^3)^{1/2}$).

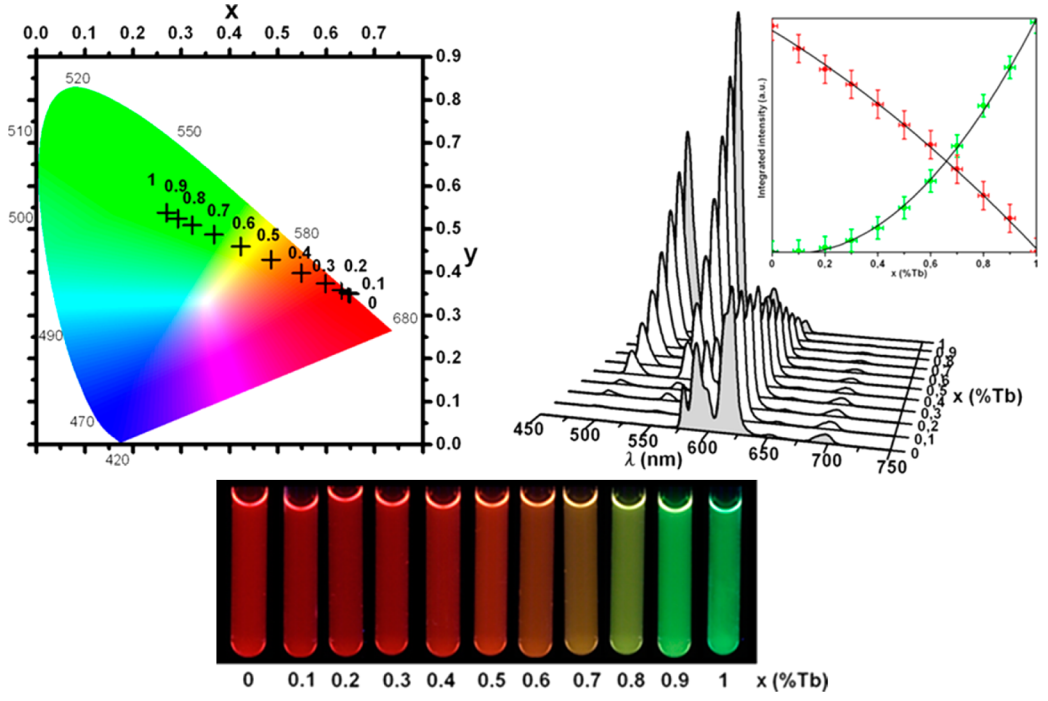

Figure 8. (upper left) Colorimetric coordinates under UV irradiation (λ_{exc} = 379 nm) of $\{[Eu_6]^{2+}_{1-x}[Tb_6]^{2+}_x\}$@EG with $0 \le x \le 1$. (upper right) Luminescence spectra of $\{[Eu_6]^{2+}_{1-x}[Tb_6]^{2+}_x\}$@EG with $0 \le x \le 1$. λ_{exc} = 379 nm. (inset) Dependence with x of the integration of Eu^{3+} transitions ($^5D_0 \rightarrow {}^7F_J$, J = 0, 1, 2, 3, 4) and Tb^{3+} transitions ($^5D_0 \rightarrow {}^7F_J$, J = 6, 5, 4, 3) in red and green, respectively. (lower) Pictures under UV irradiation of $\{[Eu_6]^{2+}_{1-x}[Tb_6]^{2+}_x\}$@EG with $0 \le x \le 1$ (λ_{exc} = 365 nm).

DOI: 10.1021/acs.inorgchem.5b00947
Inorg. Chem. 2015, 54, 6043−6054

for direct excitation of both Eu^{3+} and Tb^{3+} ($^5L_7 \leftarrow {}^7F_0$ and $^5D_3 \leftarrow {}^7F_6$ transitions, respectively).

These results suggest that there is very little energy transfer between Tb^{3+} and Eu^{3+}. Actually, contrary to what is observed when efficient intermetallic energy transfer occurs,[44,63,90−92] colorimetric coordinates and intensities of the luminescence peaks vary almost linearly with x. This confirms that lanthanide ions that belong to different hexanuclear complexes are quite far from each other even if they belong to the same nanoaggregate.

On the basis of all these experiments, we propose a model that is schematized in Scheme 1. In this model, hexanuclear complexes are separated and solvated by EG molecules. There is a dynamic exchange between water molecules and EG molecules. Coordinated molecules are also involved in a complex and dynamic network of hydrogen bonds with "solvating" EG or water molecules that are located between the hexanuclear cores. This hydrogen-bond network is strong enough for providing quite good stability to the nanoaggregates. This model addresses all the experimental observations we made during this study. To the best of our knowledge this kind of nanoaggregate of polynuclear lanthanide-based complex has never been reported before.

Scheme 1. Structural Model Proposed for $[Ln_6]^{2+}$@EG Nanoaggregates

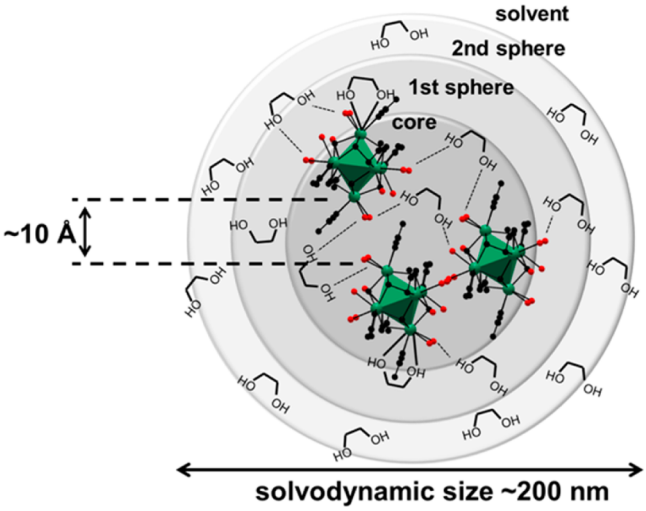

Chemical Robustness of $[Ln_6]^{2+}$@EG Aggregates toward Dilution by Another Solvent. For estimating the chemical robustness of these entities we worked with the Eu-based species and used its characteristic luminescence spectrum as a fingerprint. First we studied, by luminescence spectroscopy, the stability of a saturated $[Eu_6]^{2+}$@EG solution (C_0) toward its dilution by another solvent. Tested solvents were ethanol, dimethyl sulfoxide (DMSO), butan-1-ol, and dimethylformamide (DMF). As a matter of example, the luminescence spectra of saturated $[Eu_6]^{2+}$@EG solutions diluted in ethanol are reported in Supporting Information, Figure S7. This experiment clearly demonstrates that hexanuclear complexes are not destroyed upon a dilution by 10 in ethanol. The perfect linear variation of the intensity of the spectra with dilution (Supporting Information, Figure S7) indicates that there is no turbidity apparition. We also followed by luminescence spectroscopy the stability versus time of $[Eu_6]^{2+}$@EG solutions diluted by ethanol, butan-1-ol, DMF, and DMSO in EG/solvent ratio equal to 1:1. These experiments demonstrate that in all cases the solutions are perfectly stable over several weeks. As a matter of example, the stability of $[Eu_6]^{2+}$@EG in a mixture of EG/ethanol 1:1 over more than 36 h is reported Supporting Information, Figure S8.

These results suggest that the nanoaggregates are quite stable and that the hexanuclear entities are protected by a sort of EG shell. On the contrary, as shown in Supporting Information, Table S5, hexanuclear entities are destroyed rapidly in pure DMF or DMSO media. This long time stability in ethanol is accompanied by a high thermal stability. Actually EG/ethanol 1:1 is liquid from −50 to +100 °C, and hexanuclear complexes are not destroyed before 200 °C.[41] On the opposite, this protection is not efficient enough toward water and only slightly delays the decomposition in EG/water 1:1 medium (see Supporting Information, Figure S9). Indeed, after only 4 h, the luminescence spectrum is modified and $Eu(OH)_3$ precipitates.

To verify the assumption of the existence of a protecting shell made of EG molecules, we studied the variation of the size distribution of the nanoaggregates versus dilution by ethanol. Results of this study are reported in Figure 9.

This study shows that at low dilution ($C_0/2 \leq C \leq C_0$), the average particle size decreases abruptly. This suggests a "cutting" of the nanoaggregates that can be related to a better affinity of hexanuclear complexes for ethanol. We assume that when monofunctional ethanol molecules substitute some

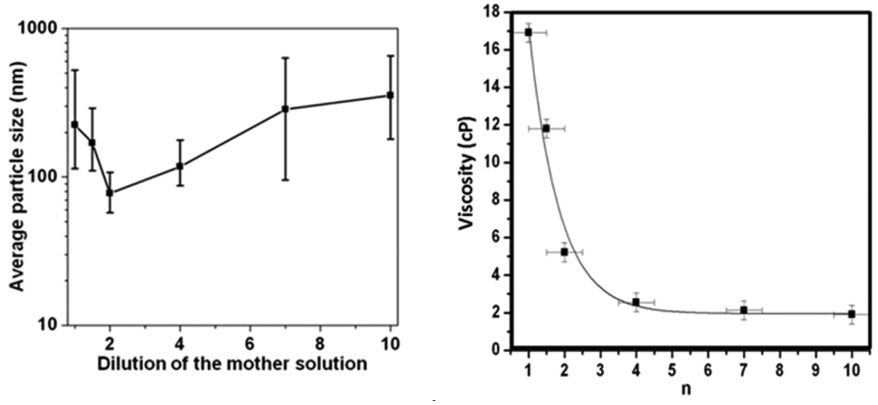

Figure 9. (left) Average particle size of $[Eu_6]^{2+}$@EG vs dilution by ethanol of the initial saturated solution. (right) Viscosity vs dilution of the different mixtures at 20 °C. Numerical values are tabulated in Supporting Information, Table S5.

DOI: 10.1021/acs.inorgchem.5b00947
Inorg. Chem. 2015, 54, 6043−6054

bifunctional EG molecules some "bridges" break up and nanoaggregates are fragmented. When dilution becomes greater, the medium is essentially constituted of ethanol in which the hexanuclear complexes present little solubility. Therefore, nanoaggregates tend to coalesce. Whatever the mechanism is, this study reveals that even in solution diluted by 10, hexanuclear complexes still exist as nanoaggregates.

Therefore, it is possible to prepare solutions of nanoaggregates that are stable for a long time over a large temperature range and that exhibit tunable luminescence properties (by mixing different hexanuclear complexes in the nanoaggregates). This could be of interest as far as luminescent solutions are needed (for fight against counterfeiting or for the design of lighting surfaces, for example). However, the systems described above suffer from a severe drawback for potential industrial application: their luminance is low, and they present no antenna effect that could allow one to excite several different hexanuclear complexes with only one excitation wavelength.

$[Ln_6]^{2+}$@HBA. To overcome this drawback, we used 2-hydroxybenzyl alcohol, hereafter symbolized by HBA, instead of EG because: (i) HBA presents two alcohol functions as EG does; (ii) HBA is flexible because of its sp^3 C; and (iii) its phenyl group may provide an antenna effect.

Concentrated solutions in ethanol of $[Ln_6]^{2+}$@HBA (C_0 = 0.006 mol L^{-1}) were prepared. Despite great efforts it has not been possible to obtain single crystal of sufficient quality for X-ray crystal structure determination. Powder X-ray diffraction patterns of the solids that were obtained by evaporation to dryness revealed that the hexanuclear complexes are not destroyed by dissolution or evaporation of the solvent.

Liquid-state ^{1}H NMR spectra of HBA and $[Y_6]^{2+}$@HBA were recorded in deuterated methanol (Supporting Information, Figure S10). These spectra clearly show that there is an interaction between the ligand and the rare earth ion. Actually, some peaks that correspond to aromatic protons are shifted toward lower fields, which indicates a decreasing of the electronic density of the protons because of Y^{3+} ions that are electro-attractive. Broadening of the observed experimental peaks suggests the coexistence in solution of different states of the HBA ligand. These states should likely correspond to free and interacting varieties of the aromatic species.

A DOSY[93,94] NMR experiment was also done (Supporting Information, Figure S11). This technique allows the estimation of the diffusion coefficient D of a compound in solution and, using the Stokes−Einstein relationship, to calculate the solvodynamic radius of this compound:

$$D = \frac{k_B T}{6\pi\eta r_H} \quad (2)$$

where k_B is the Boltzmann constant, T is the temperature (K), η is the viscosity of the medium (Pa·s), and r_H is the solvodynamic radius.[95,96]

The measured values for HBA are in good agreement with what was expected on the basis of the available X-ray diffraction data (see Table 3). The diffusion coefficient of the ligand in the presence of the hexanuclear complex is present and is smaller, which indicates that the ligand is associated with a bigger entity that diffuses slower. This suggests that the ligand is coordinated to the hexanuclear complex.

From Table 3, notice that the deduced solvodynamic radius is a little smaller than what could be expected from $r_{X\text{-ray}}$ and considering the second sphere provided by ligand and solvent molecules. In fact, the measured diffusion coefficient is relative to different contributions in equilibrium (free and interacting varieties of the aromatic ligand as assumed previously on the basis of ^{1}H NMR spectrum of $[Y_6]^{2+}$@EG). Thus, it can be seen as a mean value of each diffusion coefficient. The experimental r_H value is consequently a bit underestimated.

Table 3. Diffusion Coefficients and Solvodynamic Radii of HBA and $[Y_6]^{2+}$@HBA in CD_3OD

	1×10^{10} D (m^2 s^{-1})	r_H (Å)[b]	$r_{X\text{-ray}}$ (Å)[a]
HBA	11.021 ± 2%	3.28	3.33 from ref 97
$[Y_6]^{2+}$@HBA	5.296 ± 2%	6.84	6.2 $[Y_6]^{2+}$ alone from ref 27

[a] $r_{X\text{-ray}}$ is the radius deduced from the X-ray crystal structure. The radius is the radius of the sphere that presents the same volume than the volume of the cell divided by Z. [b] η = 0.602 mPa s from refs 98 and 99.

This type of study has been realized only once before for a rare earth-based poly nuclear complex in solution.[100] However, it is quite often used for the characterization of supramolecular complexes. Actually, there is a relationship between the diffusion coefficient D (m^2 s^{-1}) and the molecular weight MW (g mol^{-1}):[101]

$$D \propto \sqrt[3]{v \times MW} \quad (3)$$

where ν is the specific volume (m^3 g^{-1}), and where the proportionality coefficient depends on the operating conditions.

Here, the specific volume was estimated as the inverse of the crystallographic density (0.42 cm^3 g^{-1}) for HBA and as the inverse of the crystallographic density of $[Y_6]^{2+}$ (0.75 cm^3 g^{-1}) for $[Y_6]^{2+}$@HBA. With this assumption, the molecular weight of $[Y_6]^{2+}$@HBA is found to be 1998 g mol^{-1}, which corresponds to 6 HBA ligands per hexanuclear core. This value is only a rough estimation that has been made on the basis of quite abrupt assumption. Nevertheless, it is in good agreement with what could be expected.

Liquid-state UV−vis absorption spectra of HBA, $[Tb_6]^{2+}$@HBA, and $[Yb_6]^{2+}$@HBA were measured in diluted ethanolic solutions (0.6 mmol L^{-1}). HBA absorption spectrum shows two absorption bands: a broad band between 250 and 300 nm and a narrower one centered at 230 nm (Supporting Information, Figure S12). In presence of hexanuclear complexes absorption spectra are modified: absorption bands become narrower and are red-shifted. More unexpected is the appearance of a new weak absorption band between 350 and 400 nm. This phenomenon tends to confirm that HBA coordinates with hexanuclear complexes.

To estimate the energies of the first excited singlet and triplet states, a liquid-state UV−vis absorption spectrum and bidimensional diagrams excitation/emission of $[Gd_6]^{2+}$@HBA in ethanol were recorded (Supporting Information, Figure S13). These spectra confirm that $[Gd_6]^{2+}$@HBA exhibits two distinct emissive triplet states that correspond to two distinct singlet/triplet states systems. For both systems the lowest excited singlet and triplet states were estimated, respectively, by referring to the wavelengths of the UV−vis absorbance edges (S_1: 365 nm ~27 400 cm^{-1} and S_2: 306 nm ~32 700 cm^{-1}) and to the shortest wavelength phosphorescent bands (T_1: 430 nm ~23 250 cm^{-1} and T_2: 330 nm ~31 250 cm^{-1}) of $[Gd_6]^{2+}$@HBA.[63,102−104] According to Reinhoudt's empirical rules,[105] the intersystem crossing is most efficient when the energy gap

DOI: 10.1021/acs.inorgchem.5b00947
Inorg. Chem. 2015, 54, 6043−6054

between singlet and excited states is ~5000 cm^{-1}. Therefore, according to this rule, intersystem crossing is more efficient for system 1 ($\Delta E(S_1 - T_1)$ = 4150 cm^{-1}) than for system 2 ($\Delta E(S_2 - T_2)$ = 1450 cm^{-1}) for which other de-excitation mechanisms can occur (vibrationally assisted). Liquid-state excitation and emission spectra were recorded for $[Ln_6]^{2+}$@HBA with Ln = Sm, Eu, Tb, and Dy in ethanol (Figure 10).

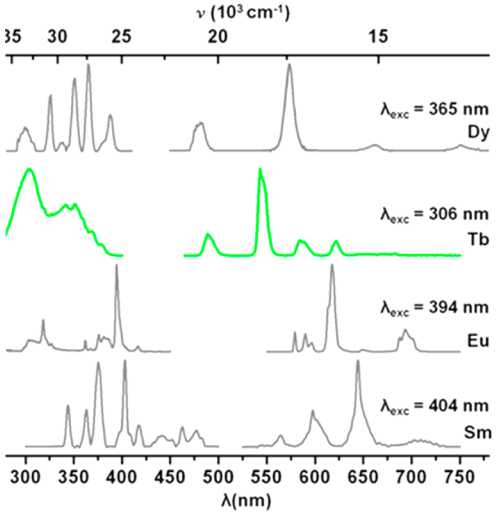

Figure 10. Liquid-state excitation and emission spectra for $[Ln_6]^{2+}$@HBA with Ln = Sm, Eu, Tb, and Dy in ethanol. The more intense wavelengths in the excitation spectra were chosen as excitation wavelengths for the corresponding emission spectra.

From this figure, notice that only the Tb-containing compound presents two intense excitation bands that correspond to both excited triplet states of the ligand. This indicates that both singlet/triplet systems of the ligand provide an antenna effect toward the Tb-based compound. This is in agreement with Latva's empirical rules[106,107] that predict that energy of the excited triplet state greater than 22 500 cm^{-1} favors a good ligand-to-metal energy transfer. Therefore, both triplet states are efficient, but triplet T_1 (23 250 cm^{-1}) is less favorable, probably because of back-transfer. Emission spectrum (Figure 10) was recorded using system 2 (λ_{exc} = 310 nm). Emission spectrum features the characteristic Tb^{3+} $^5D_4 \rightarrow {}^7F_J$ (J = 0−6) transitions and is dominated by the green $^5D_4 \rightarrow {}^7F_5$ transition centered at 545 nm (colorimetric coordinates of $[Tb_6]^{2+}$@HBA in ethanol under UV irradiation are x = 0.35(1) and y = 0.59(1)). Under UV irradiation, the ethanolic solution of $[Tb_6]^{2+}$@HBA (C_0 = 0.006 mol L^{-1}) exhibits quite intense green luminescence (0.11 Cd m^{-2}). Molar luminance (18 Cd·m^{-2} mol^{-1} L) is more intense than that of $[Tb_6]^{2+}$@CH_3CN (which is not measurable) and even better than that of $[Tb_6]^{2+}$@EG (12 Cd·m^{-2} mol^{-1} L). See Supporting Information, Figure S14 for a comparison between the different solutions. Quantum yield and luminescence lifetimes were also measured: Q_{Tb}^{ligand} = 14(1) % and τ_0 = 0.70(3) ms.

$[Eu_6]^{2+}$@HBA in ethanol presents no antenna effect. Actually, Latva's empirical rules stipulate that efficient ligand-to-metal energy transfer is ensured by ligands that present an excited triplet state energy comprised between 20 000 and 23 000 cm^{-1}. Therefore, the T_2 triplet state is too high (31 250 cm^{-1}), the T_1 triplet state (23 250 cm^{-1}) is just on the limit, and back-transfer can occur. However, it is well-known that for easily reducible lanthanide ions a redox-based mechanism can operate in which the first step is a photoinduced electron transfer (PET) from the ligand to the lanthanide ion.[5,108] This mechanism is known for being efficient when $-NH_2$ or $-OH$ electron donor groups are present in the vicinity of the lanthanide ion.[109] Both quenching mechanisms (back-transfer and PET) are highly thermodependent. Therefore, we recorded excitation spectra for $[Eu_6]^{2+}$@HBA in ethanol at room temperature and at 77 K. These spectra actually present a strong dependence versus temperature (Supporting Information, Figure S15). However, PET is most likely the dominant mechanism since emission occurs under direct excitation of the lanthanide ion (Figure 10).[90,110] At last, this emission spectrum, recorded under direct excitation of the ligand, presents strong similarities with emission spectrum of $[Eu_6]^{2+}$@EG (see Supporting Information, Figure S16). This suggests that the neighborhood of Eu^{3+} ions is probably quite similar in both compounds.

Excitation and emission spectra were also recorded for $[Ln_6]^{2+}$@HBA in ethanol with Ln = Nd, Er, or Yb, that is, for compounds that involve lanthanide ions that usually present a luminescence in the infrared domain. Latva's rule are no more valid for these lanthanide ions, and it has been demonstrated that energy transfer is ensured by other mechanisms such as phonon-assisted process[111] for Yb(III) ions, for example. All the excitation spectra are identical and show an excitation band that corresponds to the ligand (λ_{exc} = 365 nm) (Figure 11).

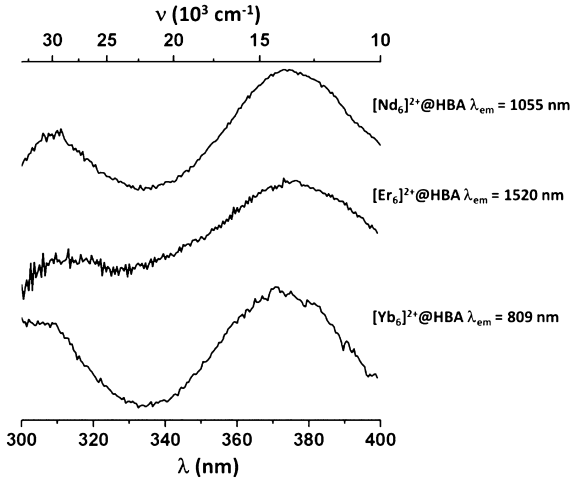

Figure 11. Excitation spectra of $[Ln_6]^{2+}$@HBA in ethanol with Ln = Nd, Er, or Yb.

■ CONCLUSIONS AND OUTLOOKS

In this paper, we have demonstrated that hexanuclear complexes can be stabilized as nanoaggregates by solvation with a polyol such as EG. These nanoaggregates have been structurally characterized, and it has been proved that they are chemically stable and that solutions can be made that remain liquid over a large temperature range. We have also demonstrated that the same strategy can be used with ligands that present an antenna effect. This is of particular interest as far as liquids that exhibit complex luminescence properties are targeted. Actually, hexanuclear complexes have already been shown to present original luminescence properties in the solid state.[44] The results described in this paper allow one to expect similar properties in the liquid state. These properties could be

DOI: 10.1021/acs.inorgchem.5b00947
Inorg. Chem. 2015, 54, 6043−6054

interesting for surface lighting or for tagging liquids against counterfeiting.

Obviously, the systems described in this paper are not optimized and only constitute a proof of concept. Preliminary tests show that this synthetic strategy can be extended to a wide number of polyols. System for direct industrial application should present high luminance and offer the possibility of tuning the emission by playing with different energy transfer processes (ligand-to-metal, metal-to-metal, up- or down-conversion, etc.). Therefore, industrially interesting systems should be constituted by heteronuclear complexes and a polyol that provides an efficient antenna effect. Our group is currently working along this line.

■ ASSOCIATED CONTENT

Supporting Information

Experimental and computational details; solubility and stability of an Er-based hexanuclear complex in various dry organic solvents; solid-state UV−vis absorption spectra for $[Ln_6O(OH)_8(NO_3)_6(H_2O)_n]\cdot 2NO_3\cdot 2H_2O$ with n = 12 for Ln = Sm−Lu and Y and n = 14 for Ln = Nd; excitation and emission spectra for $[Ln_6O(OH)_8(NO_3)_6(H_2O)_n]\cdot 2NO_3\cdot 2H_2O$ with n = 12 for Ln = Sm−Lu and Y and n = 14 for Ln = Nd; powder X-ray diffraction patterns of $[Y_6O(OH)_8(NO_3)_6(H_2O)_{12}]\cdot 2NO_3\cdot 2H_2O$; ESI-MS spectrum of $[Eu_6]^{2+}$@EG in an EG/propan-2-on solution (1:100); liquid state UV−vis absorption spectra for $[Ln_6]^{2+}$@EG for Ln = Nd−Lu; excitation and emission spectra for $[Ln_6]^{2+}$@EG, where Ln = Sm, Eu, Tb, Dy, or Tm; integrated intensities of room-temperature luminescence spectra of a $Eu(NO_3)_3\cdot 6H_2O$ solution in EG and of $[Eu_6]^{2+}$@EG; normalized intensities of $[Eu_6(\mu_6\text{-}O)(\mu_3\text{-}OH)_8(H_2O)_{12}(NO_3)_6]\cdot 2NO_3\cdot 2H_2O$ (77 K) solid-state luminescence spectrum and of $[Eu_6]^{2+}$@EG liquid-state luminescence spectrum; luminescence spectra of $[Eu_6]^{2+}$@EG solutions diluted by ethanol; intensity of the peak centered at 620 nm ($^5D_0 \rightarrow {}^7F_2$ transition) in the luminescence spectrum of $[Eu_6]^{2+}$@EG in a mixture of EG/ethanol 1:1; luminescence spectra of $[Eu_6]^{2+}$@EG in EG and in a mixture of EG/water 1:1 after 4 h; liquid-state ^{1}H NMR spectra of HBA and $[Y_6]^{2+}$@HBA; DOSY NMR spectra and experimental details of HBA and $[Y_6]^{2+}$@HBA; liquid-state UV−vis absorption spectra of HBA, $[Tb_6]^{2+}$@HBA, and $[Yb_6]^{2+}$@HBA in ethanol (0.6 mmol L^{-1}); liquid-state UV−vis absorption spectrum of HBA in ethanol; pictures under UV irradiation of $[Tb_6]^{2+}$@CH3CN, $[Tb_6]^{2+}$@HBA in ethanol, and $[Tb_6]^{2+}$@EG illustrating the intrinsic luminance of the different solutions; excitation spectra for $[Eu_6]^{2+}$@HBA in ethanol at room temperature and 77 K, λ_{em} = 620 nm; liquid-state emission spectra of $[Eu_6]^{2+}$@HBA in ethanol and $[Eu_6]^{2+}$@EG and solid-state emission spectrum of $[Eu_6(\mu_6\text{-}O)(\mu_3\text{-}OH)_8(H_2O)_{12}(NO_3)_6]\cdot 2NO_3\cdot 2H_2O$; relative contents of Eu^{3+} and Tb^{3+} in $\{[Eu_6]^{2+}_{1-x}[Tb_6]^{2+}_x\}$@EG with $0 \le x \le 1$; viscosity of $[Eu_6]^{2+}$@EG versus dilution of the different mixtures. The Supporting Information is available free of charge on the ACS Publications website at DOI: 10.1021/acs.inorgchem.5b00947.

■ AUTHOR INFORMATION

Corresponding Authors

*E-mail: olivier.guillou@insa-rennes.fr. (O.G.)
*E-mail: guillaume.calvez@insa-rennes.fr. (G.C.)

Present Address

⊥CNRS, LINK, UMI 3629, National Institute of Material Science, 1−1 Namiki, 305−0044, Tsukuba, Japan.

Notes

The authors declare no competing financial interest.

■ ACKNOWLEDGMENTS

M. J. Laisney (Université de Paris XI—Orsay) and Dr. V. Dorcet (CMEBA—Université de Rennes 1) are acknowledged for TEM measurements. M. P. Jehan (CRMPO—Université de Rennes 1) is acknowledged for ESI-MS experiments. Financial support from the IR-RMN-THC Fr3050 CNRS for conducting the research is gratefully acknowledged. Dr F. Le Natur thanks Région Bretagne for financial support. Computations were performed using HPC resources from GENCI-CINES and GENCI-IDRIS (Grant No. 2014-80649), which are gratefully acknowledged.

■ REFERENCES

(1) Eliseeva, S. V.; Bünzli, J. C. G. *New J. Chem.* **2011**, *35*, 1165−1176.
(2) Binnemans, K. *Chem. Rev.* **2009**, *109*, 4283−4374.
(3) You, H.; Fang, J.; Xuan, Y.; Ma, D. *Mater. Sci. Eng., B* **2006**, *131*, 252.
(4) Maas, H.; Currao, A.; Gion, C. *Angew. Chem., Int. Ed.* **2002**, *41*, 2495.
(5) Bünzli, J.-C. G. *Chem. Rev.* **2010**, *111*, 2729−2755.
(6) Comby, S.; Bünzli, J. C. G.; Gschneider, K. A.; Pecharsky, V. K., Lanthanide Near-Infrared Luminescence in Molecular Probes and Devices. In *Handook on the Physics and Chemistry of Rare Earths;* Elsevier: Amsterdam, 2007; Vol. *37*, pp 1−353.
(7) Bünzli, J. C. G.; Eliseeva, S. V. Basics of Lanthanide Photophysics. In *Lanthanide Luminescence;* Hänninen, P.; Härmä, H., Eds.; Springer: Berlin, Germany, 2010; pp 1−45.
(8) Gai, S.; Li, C.; Yang, P.; Lin, J. D. *Chem. Rev.* **2014**, *114*, 2243−2389.
(9) Daiguebonne, C.; Kerbellec, N.; Guillou, O.; Bünzli, J. C. G.; Gumy, F.; Catala, L.; Mallah, T.; Audebrand, N.; Gérault, Y.; Bernot, K.; Calvez, G. *Inorg. Chem.* **2008**, *47*, 3700−3708.
(10) Shen, J.; Sun, L.-D.; Yan, C.-H. *Dalton Trans.* **2008**, *42*, 5687−5697.
(11) Kerbellec, N.; Catala, L.; Daiguebonne, C.; Gloter, A.; Stephan, O.; Bünzli, J. C. G.; Guillou, O.; Mallah, T. *New J. Chem.* **2008**, *32*, 584−587.
(12) Alexandropoulos, D. I.; Mukherjee, S.; Papatriantafyllopoulou, C.; Raptopoulou, C. P.; Psycharis, V.; Bekiari, V.; Christou, G.; Stamatatos, T. C. *Inorg. Chem.* **2011**, *50*, 11276−11278.
(13) Andrews, P. C.; Beck, T.; Fraser, B. H.; Junk, P. C.; Massi, M.; Moubaraki, B.; Murray, K. S.; Silberstein, M. *Polyhedron* **2009**, *28*, 2123−2130.
(14) Babai, A.; Mudring, A.-V. *Z. Anorg. Allg. Chem.* **2006**, *632*, 1956−1958.
(15) Baril-Robert, F.; Petit, S.; Pilet, G.; Chastanet, G.; Reber, C.; Luneau, D. *Inorg. Chem.* **2010**, *49*, 10970−10976.
(16) Bürgstein, M. R.; Gamer, M. T.; Roesky, P. W. *J. Am. Chem. Soc.* **2004**, *126*, 5213−5218.
(17) Costes, J.-P.; Dahan, F.; Nicodeme, F. *Inorg. Chem.* **2001**, *40*, 5285−5287.
(18) de Villiers, J. P. R.; Boeyens, J. C. A. *Acta Crystallogr., Sect. B* **1971**, *27*, 692−702.
(19) Fang, W.-H.; Cheng, L.; Huang, L.; Yang, G.-Y. *Inorg. Chem.* **2013**, *52*, 6−8.
(20) Gao, Y.; Xu, G.-F.; Zhao, L.; Tang, J.; Liu, Z. *Inorg. Chem.* **2009**, *48*, 11495−11497.
(21) Giester, G.; Zak, Z.; Unfried, P. *J. Alloys Compd.* **2009**, *481*, 116−128.
(22) Gu, X.; Xue, D. *Inorg. Chem.* **2007**, *46*, 3212−3216.

DOI: 10.1021/acs.inorgchem.5b00947
Inorg. Chem. 2015, 54, 6043−6054

(23) Huang, L.; Han, L.; Feng, W.; Zheng, L.; Zhang, Z.; Xu, Y.; Chen, Q.; Zhu, D.; Niu, S. *Cryst. Growth Des.* **2010**, *10*, 2548−2552.
(24) Kang, J.-G.; Yoon, S.-K.; Sohn, Y.; Kim, J.-G.; Kim, Y.-D.; Suh, I.-H. *J. Chem. Soc., Dalton Trans.* **1999**, 1467−1474.
(25) Kong, X.-J.; Wu, Y.; Long, L.-S.; Zheng, L.-S.; Zheng, Z. *J. Am. Chem. Soc.* **2009**, *131*, 6918−6919.
(26) Li, X.-L.; He, L.-F.; Feng, X.-L.; Song, Y.; Hu, M.; Han, L.-F.; Zheng, X.-J.; Zhang, Z.-H.; Fang, S.-M. *CrystEngComm* **2011**, *13*, 3643−3645.
(27) Mahé, N.; Guillou, O.; Daiguebonne, C.; Gérault, Y.; Caneschi, A.; Sangregorio, C.; Chane-Ching, J. Y.; Car, P. E.; Roisnel, T. *Inorg. Chem.* **2005**, *44*, 7743−7750.
(28) Paluch, M.; Slepokura, K.; Lis, T.; Lisowski, J. *Inorg. Chem. Commun.* **2011**, *14*, 92−95.
(29) Petit, S.; Baril-Robert, F.; Pilet, G.; Reber, C.; Luneau, D. *Dalton Trans.* **2009**, 6809−6815.
(30) Roesky, P. W.; Canseco-Melchor, G.; Zulys, A. *Chem. Commun.* **2004**, 738−739.
(31) Thielemann, D. T.; Wagner, A. T.; Rösch, E.; Kölmel, D. K.; Heck, J. G.; Rudat, B.; Neumaier, M.; Feldmann, C.; Schepers, U.; Bräse, S.; Roesky, P. W. *J. Am. Chem. Soc.* **2013**, *135*, 7454−7457.
(32) Wang, R.; Liu, H.; Carducci, M. D.; Jin, T.; Zheng, C.; Zheng, Z. *Inorg. Chem.* **2001**, *40*, 2743−2750.
(33) Wang, R.; Selby, H. D.; Liu, H.; Carducci, M. D.; Jin, T.; Zheng, Z.; Anthis, J. W.; Staples, R. J. *Inorg. Chem.* **2002**, *41*, 278−286.
(34) Weng, D.; Zheng, X.; Jin, L. *Eur. J. Inorg. Chem.* **2006**, 4184−4190.
(35) Zheng, X. J.; Jin, L. P.; Gao, S. *Inorg. Chem.* **2004**, *43*, 1600−1602.
(36) Zheng, Z. *Chem. Commun.* **2001**, 2521−2529.
(37) Zheng, Z.; Wang, R. *Comments Inorg. Chem.* **2000**, *22*, 1−30.
(38) Calvez, G.; Guillou, O.; Daiguebonne, C.; Car, P.-E.; Guillerm, V.; Gérault, Y.; Dret, F. L.; Mahé, N. *Inorg. Chim. Acta* **2008**, *361*, 2349−2356.
(39) Calvez, G.; Bernot, K.; Guillou, O.; Daiguebonne, C.; Caneschi, A.; Mahé, N. *Inorg. Chim. Acta* **2008**, *361*, 3997−4003.
(40) Chane-Ching, J. Y.; Guillou, O.; Mahé, N. Cluster de praséodyme, dispersion aqueuse et dispersion en milieu solvant de ce cluster et leurs procédés de séparation. FR 2 847 248 6-A1, 2002.
(41) Calvez, G.; Daiguebonne, C.; Guillou, O.; Pott, T.; Méléard, P.; Le Dret, F. *C. R. Chim.* **2010**, *13*, 715−730.
(42) Calvez, G.; Daiguebonne, C.; Guillou, O.; Le Dret, F. *Eur. J. Inorg. Chem.* **2009**, 3172−3178.
(43) Calvez, G.; Daiguebonne, C.; Guillou, O. *Inorg. Chem.* **2011**, *50*, 2851−2858.
(44) Le Natur, F.; Calvez, G.; Daiguebonne, C.; Guillou, O.; Bernot, K.; Ledoux, J.; Le Polles, L.; Roiland, C. *Inorg. Chem.* **2013**, *52*, 6720−6730.
(45) Calvez, G.; Guillou, O.; Le Natur, F. Procédé de marquage d'au moins un matériau comprenant une matrice solide ou liquide, organique ou minérale, et matériau correspondant. FR2995316-A1, 2012.
(46) Guillou, O.; Daiguebonne, C.; Calvez, G.; Le Dret, F.; Car, P. E. *J. Alloys Compd.* **2008**, *451*, 329−333.
(47) Pearson, R. G. *Coord. Chem. Rev.* **1990**, 403−425.
(48) Ninni, L.; Camargo, M. S.; Meirelles, A. J. A. *J. Chem. Eng. Data* **2000**, *45*, 654−660.
(49) Marcolli, C.; Peter, T. *Atmos. Chem. Phys.* **2005**, *5*, 1545−1555.
(50) Yang, L.; Zhao, Y.; Tian, W.; Jin, X.; Weng, S.; Wu, J. *Carbohydr. Res.* **2001**, *330*, 125−130.
(51) Su, Y.; Yang, L.; Wang, Z.; Jin, X.; Weng, S.; Wu, J. *Carbohydr. Res.* **2006**, *341*, 75−83.
(52) Yang, L.; Hua, X.; Xue, J.; Pan, Q.; Yu, L.; Li, W.; Xu, Y.; Zhao, G.; Liu, L.; Liu, K.; Chen, J. E.; Wu, J. *Inorg. Chem.* **2012**, *51*, 499−510.
(53) Yu, L.; Hua, X.; Pan, Q.; Yang, L.; Xu, Y.; Zhao, G.; Wang, H.; Wu, J.; Liu, K.; Chen, J. E. *Carbohydr. Res.* **2007**, *346*, 2278−2284.
(54) Naruke, H.; Yamase, T.; Ohno, H. *J. Alloys Compd.* **1997**, *261*, 140−144.
(55) Angyal, S. J.; Craig, D. C. *Carbohydr. Res.* **1993**, *241*, 1−8.
(56) Su, Y.; Yang, L.; Xu, Y.; Wang, Z.; Weng, S.; Yan, C.; Wang, D.; Wu, J. *Inorg. Chem.* **2007**, *46*, 5508−5517.
(57) Delangle, P.; Husson, C.; Lebrun, C.; Pecaut, J.; Vottero, P. J. A. *Inorg. Chem.* **2001**, *40*, 2953−2962.
(58) Liu, Y.-S.; Tang, M.-F.; Lii, K.-H. *Dalton Trans.* **2009**, 9781−9786.
(59) Nakajima, A.; Itoh, S.; Kurihara, M.; Sakamoto, M.; Yoshioka, D.; Mikuriya, M.; Hamakawa, S.; Mizukami, F. *Inorg. Chem. Commun.* **2008**, *11*, 323−325.
(60) Jensen, C. M.; Lee, D. W. *J. Chem. Educ.* **2000**, *77*, 629.
(61) Desreux, J. F. In *Lanthanide Probes in Life, Chemical and Earth Sciences;* Choppin, G. R.; Bünzli, J. C. G., Eds.; Elsevier: Amsterdam, 1989; p 43.
(62) Lyle, S. J.; Rahman, M. M. *Talanta* **1963**, 1177−1182.
(63) Haquin, V.; Etienne, M.; Daiguebonne, C.; Freslon, S.; Calvez, G.; Bernot, K.; Le Polles, L.; Ashbrook, S. E.; Mitchell, M. R.; Bünzli, J. C. G.; Guillou, O. *Eur. J. Inorg. Chem.* **2013**, 3464−3476.
(64) Mitchell, M. R.; Carnevale, D.; Orr, R.; Whittle, K. R.; Ashbrook, S. E. *J. Phys. Chem. C* **2012**, *116*, 4273−4286.
(65) Reader, S. W.; Mitchell, M. R.; Johnston, K. E.; Pickard, C. J.; Whittle, K. R.; Ashbrook, S. E. *J. Phys. Chem. C* **2009**, *113*, 18874−18883.
(66) Ashbrook, S. E.; Whittle, K. R.; Lumpkin, G. R.; Farnan, I. *J. Phys. Chem. B* **2006**, *110*, 10358−10364.
(67) Roger, J.; Babizhetsky, V.; Cordier, S.; Bauer, J.; Hiebl, K.; Le Polles, L.; Ashbrook, S. E.; Halet, J. F.; Guerin, R. *J. Solid State Chem.* **2005**, *178*, 1854−1866.
(68) Löble, M. W.; Casimiro, M.; Thielemann, D. T.; Oña-Burgos, P.; Fernández, I.; Roesky, P. W.; Breher, F. *Chem.—Eur. J.* **2012**, *18*, 5325−5334.
(69) White, R. E.; Hanusa, T. P. *Organometallics* **2006**, *25*, 5621−5630.
(70) Piotto, M.; Bourdonneau, M.; Elbayed, K.; Wieruszeski, J.-M.; Lippens, G. *Magn. Reson. Chem.* **2006**, *44*, 943−947.
(71) Patiny, L.; Borel, A. *J. Chem. Inf. Model.* **2013**, *53*, 1223−1228.
(72) Liu, G.; Liu, T.; Mal, S. S.; Kortz, U. *J. Am. Chem. Soc.* **2006**, *128*, 10103−10110.
(73) Shen, M.; Sun, Y.; Han, Y.; Yao, R.; Yan, C. *Langmuir* **2008**, *24*, 13161−13167.
(74) Balch, R. T. *Ind. Eng. Chem. Anal. Ed.* **1931**, *3*, 124−127.
(75) Furet, E.; Costuas, K.; Rabiller, P.; Maury, O. *J. Am. Chem. Soc.* **2008**, *130*, 2180−2183.
(76) van der Voort, D.; Dirksen, G. J.; Blasse, G. *J. Phys. Chem. Solids* **1992**, *53*, 219−225.
(77) Parker, D.; Dickins, R. S.; Puschmann, H.; Crosslan, C.; Howard, J. A. K. *Chem. Rev.* **2002**, *102*, 1977−2010.
(78) Mahesh, S. K.; Prabhakar Rao, P.; Thomas, M.; Francis, T. L.; Koshy, P. *Inorg. Chem.* **2013**, *52*, 13304−13313.
(79) Stumpf, T.; Bolte, M. *Acta Crystallogr., Sect. E* **2001**, *E57*, i10−i11.
(80) Platas-Iglesias, C.; Roca-Sabio, A.; Regueiro-Figueroa, M.; Esteban-Gomez, D.; De Blas, A.; Rodriguez-Blas, T. *Curr. Inorg. Chem.* **2011**, *1*, 91−116.
(81) Hammell, J.; Buttarazzi, L.; Huang, C.-H.; Morrow, J. R. *Inorg. Chem.* **2011**, *50*, 4857−4867.
(82) Butler, S. J.; Parker, D. *Chem. Soc. Rev.* **2013**, *42*, 1652−1666.
(83) Butler, S. J.; Mc Mahon, B. K.; Pal, R.; Parker, D.; Walton, J. W. *Chem.—Eur. J.* **2013**, *19*, 9511−9517.
(84) Horrocks, W. D.; Sudnick, D. R. *J. Am. Chem. Soc.* **1979**, *101*, 334−340.
(85) Kimura, T.; Kato, Y. *J. Alloys Compd.* **1998**, *275−277*, 806−810.
(86) Kimura, T.; Kato, Y. *J. Alloys Compd.* **1995**, *225*, 284−287.
(87) Choppin, G. R.; Peterman, D. R. *Coord. Chem. Rev.* **1998**, *174*, 283−299.
(88) Supkowski, R. M.; Horrocks, W. D. *Inorg. Chim. Acta* **2002**, *340*, 44−48.
(89) Kerbellec, N.; Kustaryono, D.; Haquin, V.; Etienne, M.; Daiguebonne, C.; Guillou, O. *Inorg. Chem.* **2009**, *48*, 2837−2843.

DOI: 10.1021/acs.inorgchem.5b00947
Inorg. Chem. 2015, 54, 6043−6054

(90) Freslon, S.; Luo, Y.; Calvez, G.; Daiguebonne, C.; Guillou, O.; Bernot, K.; Michel, V.; Fan, X. *Inorg. Chem.* **2014**, *53*, 1217−1228.
(91) Luo, Y.; Zheng, Y.; Calvez, G.; Freslon, S.; Bernot, K.; Daiguebonne, C.; Roisnel, T.; Guillou, O. *CrystEngComm* **2013**, *15*, 706−720.
(92) Luo, Y.; Calvez, G.; Freslon, S.; Bernot, K.; Daiguebonne, C.; Guillou, O. *Eur. J. Inorg. Chem.* **2011**, 3705−3716.
(93) Price, W. S. *Concepts Magn. Reson.* **1998**, *10*, 197−237.
(94) Morris, K. F.; Johnson, C. S. *J. Am. Chem. Soc.* **1992**, *114*, 3139−3141.
(95) Cohen, Y.; Avram, L.; Frish, L. *Angew. Chem., Int. Ed* **2005**, *44*, 520−554.
(96) Pregosin, P. S.; Kumar, P. G. A.; Fernandez, I. *Chem. Rev.* **2005**, *105*, 2977−2998.
(97) Lemmerer, A.; Esterhuysen, C. *CrystEngComm* **2011**, *13*, 5773−5782.
(98) Holz, M.; Mao, X. A.; Seiferling, D.; Sacco, A. *J. Chem. Phys.* **1996**, *104*, 669−679.
(99) Liu, X.; Liu, Y.; Li, G.; Warmuth, R. *Angew. Chem., Int. Ed* **2006**, *45*, 901−904.
(100) Thielemann, D. T.; Fernandez, I.; Roesky, P. W. *Dalton Trans.* **2010**, *39*, 6661−6666.
(101) Hamacek, J.; Bernardinelli, G.; Fillinchuk, Y. *Eur. J. Inorg. Chem.* **2008**, 3419−3422.
(102) Shi, M.; Li, F.; Yi, T.; Zhang, D.; Hu, H.; Huang, C.-H. *Inorg. Chem.* **2005**, *44*, 8929.
(103) Prodi, L.; Maestri, M.; Ziessel, R.; Balzani, V. *Inorg. Chem.* **1991**, *30*, 3798−3802.
(104) Quici, S.; Cavazzini, M.; Marzanni, G.; Accors, i. G.; Armaroli, N.; Ventura, B.; Barigelletti, F. *Inorg. Chem.* **2005**, *44*, 529−537.
(105) Steemers, F. J.; Verboom, W.; Reinhoudt, D. N.; Van der Tol, E. B.; Verhoeven, J. W. *J. Am. Chem. Soc.* **1995**, *117*, 9408−9414.
(106) Eliseeva, S. V.; Bünzli, J. C. G. *Chem. Soc. Rev.* **2010**, *39*, 189−227.
(107) Latva, M.; Takalo, H.; Mukkala, V.-M.; Matachescu, C.; Rodriguez-Ubis, J. C.; Kankare, J. *J. Lumin.* **1997**, *75*, 149−169.
(108) Ward, M. D. *Coord. Chem. Rev.* **2007**, *251*, 1663−1677.
(109) Galaup, C.; Couchet, J.-M.; Bedel, S.; Tisnès, P.; Picard, C. *J. Org. Chem.* **2005**, *70*, 2274−2284.
(110) Fan, X.; Freslon, S.; Daiguebonne, C.; Calvez, G.; Le Polles, L.; Bernot, K.; Guillou, O. *J. Mater. Chem. C* **2014**, 5510−5525.
(111) Reinhard, C.; Gudel, H. U. *Inorg. Chem.* **2001**, *41*, 1048−1055.

DOI: 10.1021/acs.inorgchem.5b00947
Inorg. Chem. 2015, 54, 6043−6054